Satellite Assessment of Divergent Water Vapor Transport from NCEP, ERA40, and JRA25 Reanalyses over the Asian Summer Monsoon Region

Seong-Chan PARK, Byung-Ju SOHN

School of Earth and Environmental Sciences, Seoul National University, Seoul, Korea

and

Bin WANG

International Pacific Research Center, School of Ocean and Earth Science and Technology, University of Hawaii at Manoa, Honolulu, Hawaii, USA

(Manuscript received 4 January 2007, in final form 21 June 2007)

Abstract

The divergent component of water vapor transports was constructed using evaporation, precipitation, and total precipitable water estimated from the Special Sensor Microwave Imager (SSM/I). The SSM/I moisture budget parameters were then compared with those from the National Centers for Environmental Prediction (NCEP), the European Centre for Medium-Range Weather Forecasts (ECMWF) 40-year Reanalysis (ERA40), and the Japanese 25-year Reanalysis Project (JRA25) data over the Asian monsoon region for the May to September (MJJAS) period from 1988 to 2000.

The climatology of SSM/I water vapor transports clearly indicates three major water vapor sources for the Asian monsoon, i.e., the subtropical Indian Ocean and Pacific Ocean in the Southern Hemisphere, and the North Pacific Ocean. In contrast, sinks are located in the Asian summer monsoon trough, the equatorial convective zones over the Indian and western Pacific Oceans, and over the East Asian monsoon region from the northern tip of Philippine Sea to the Kuroshio extension region. These sources and sinks are linked to well-known large-scale rotational circulation features, i.e., the cross-equatorial flow associated with monsoon circulation over the Indian Ocean, the anticyclonic circulation along the western periphery of the western North Pacific High, and the cross-equatorial flow north of New Guinea. In conjunction with the fluctuation of these sources and sinks, the northward propagating climatological intraseasonal oscillations in water vapor flux convergence are evident in the South and East Asian monsoon regions in the SSM/I data.

From the comparison of water budget parameters of NCEP, ERA40, and JRA25 reanalysis with SSM/I-derived features, we found that the general features of all three reanalyses are in good agreement with those from SSM/I; however, the magnitudes of water vapor transports are comparatively weaker in all three reanalyses than what SSM/I measurements suggested. In addition, much weaker water vapor transports in three reanalyses are found in the intraseasonal oscillation signals with less distinct patterns, compared to what are inferred from the SSM/I measurements.

1. Introduction

Global reanalysis data produced independently by major operational centers, such as the National Centers for Environmental Prediction (NCEP) and the European Centre for Medium-

Corresponding author: Byung-Ju Sohn, School of Earth and Environmental Sciences, Seoul National University, NS80, Seoul, 151-747, Korea.
E-mail: sohn@snu.ac.kr

Range Weather Forecasts (ECMWF) have been widely used to examine the Earth's global hydrological cycle and to understand its associated atmospheric circulation (Trenberth and Guillemot 1995; Mo and Higgins 1996; Trenberth and Guillemot 1998; Cohen et al. 2000; Roads et al. 2002). These reanalyses are produced by assimilating the models' first guess fields to various meteorological observations. Some of the variables such as pressure, temperature, wind, and humidity are directly analyzed by the assimilation system, while others, like precipitation and evaporation, are derived products which strongly depend on the model physics and thus the model parameterization. In other words, those derived variables are model-dependent and are not fully determined by the observations. Furthermore, the water vapor balance is not warranted.

Naturally we expect uncertainties in the hydrological cycle in the reanalysis data, due to insufficient and inaccurate observations used for the reanalyses as well as deficiencies within the assimilation system. For instance, Rasmusson and Mo (1996) demonstrated that the hydrological cycle from NCEP is useful for describing general features of the atmospheric branch of the hydrological cycle. At the same time, they also showed that there are limitations in the study of continental-scale moisture budgets because of large regional terrain-related systematic biases. Consistent with this point, Trenberth and Guillemot (1998) noted a negative bias in tropical precipitation in NCEP products, suggesting a weak divergent circulation over the Tropics.

Consequently uncertainties in moisture budgets remain among various reanalyses (Annamalai et al. 1999; Newman et al. 2000) although intercomparison itself provides a means for diagnosing the performance of global analyses and climate models. To evaluate the quality of global reanalysis data, or to better understand the role of the hydrological cycle in the Earth's climate, quantitative "ground-truth" information is demanded.

The recent advent of satellites such as the Special Sensor Microwave Imager (SSM/I) onboard the Defense Meteorological Satellite Program (DMSP) satellite can provide atmospheric water budget parameters, i.e., water vapor, cloud liquid water, and precipitation, to examine the water budget in the atmosphere. The spatial and temporal homogeneity and accuracy of satellite observations offer an opportunity for a satellite-based study of the hydrological cycle, which in essence, captures all the important water budget components and water vapor transport features. Thus, it is worthwhile to compare well-known global reanalysis against SSM/I-derived water budget data, and shed light on the strengths and weaknesses of the reanalyses, as well as the ways, by which the model physics might be improved.

In this paper, we compare the divergent component of water vapor transports derived from reanalyses against SSM/I-derived parameters over the Asian summer monsoon region. The moisture sources and sinks, and their associated transport features, are important elements for understanding the monsoon precipitation and circulation. In doing so, we constructed the moisture transport field using the SSM/I retrieved precipitation and evaporation datasets for the period of 1988–2000, by applying the methodology developed by Sohn et al. (2004). The satellite-derived moisture budget parameters will then be compared with those from NCEP, ECMWF 40-year reanalysis (ERA40), and Japanese 25-year Reanalysis Project (JRA25) data. In this study, we aim to identify common features and discrepancies among various reanalyses and satellite-based results, and attempt to explain what might give rise to such discrepancies.

We describe the methodology and datasets in Section 2. Section 3 compares the derived moisture flux divergence from the satellite measurements and reanalysis data, along with radiosonde observations. In Section 4 we present geographical distributions of precipitation, evaporation, and associated divergent component of water vapor transports from the SSM/I, and from NCEP, ERA40, and JRA25 reanalyses. Climatological intraseasonal variations associated with the water vapor transport and divergence field are discussed in Section 5 and conclusions follow in Section 6.

2. Methodology and description of used datasets

The methodology used here for deriving water vapor transports over the global oceans from satellite-retrieved precipitation (P) and evapo-

ration (E) is described in detail in Sohn et al. (2004). Briefly, for a given atmospheric column, the water balance is achieved as follows:

$$\frac{\partial W}{\partial t} + \nabla \bullet \mathbf{Q} = E - P, \tag{1}$$

where W is the total amount of precipitable water, E and P are evaporation and precipitation, respectively. $\mathbf{Q}$ is the horizontal water vapor transport vector defined by

$$\mathbf{Q} = \frac{1}{g}\int_{p_0}^{p_s} q\mathbf{V}\, dp, \tag{2}$$

where g is the acceleration of gravity, q is specific humidity, $\mathbf{V}$ is the horizontal wind vector, p_s is the pressure at the surface, and p_0 is the pressure at the top of the atmosphere.

In the case of SSM/I, by separating the water vapor transport vector ($\mathbf{Q}$) into rotational ($\mathbf{Q}_R$) and divergent ($\mathbf{Q}_D$) components (Rosen et al. 1979; Chen 1985; Sohn et al. 2004) and introducing the water vapor transport potential function (Φ) we effectively remove the rotational component ($\mathbf{Q}_R$), i.e.:

$$\nabla \bullet \mathbf{Q}_D = E - P - \frac{\partial W}{\partial t} = -\nabla^2\Phi \tag{3}$$

$$\mathbf{Q}_D = -\nabla\Phi. \tag{4}$$

Equations (3) and (4) are solved for Φ by using a spectral method on a global domain with inputs of evaporation, precipitation, and total precipitable water. The used pentad mean SSM/I data are given in a $2.5^\circ \times 2.5^\circ$ grid format. Solving Eq. (3) for the SSM/I water vapor transport potential function (Φ) requires known boundary conditions for a given domain. To avoid the difficulty in specifying boundary conditions, we solve Eq. (3) over the whole globe using spherical harmonics in which boundary conditions vanish at both poles.

As in Eq. (3), the local change of W needs to be calculated for solving the water vapor flux divergence. The local change term $\left(\frac{\partial W}{\partial t}\right)$ is explicitly calculated using pentad means of total precipitable water. For the calculation of SSM/I divergent component of water vapor transports in a global domain, land areas void of SSM/I precipitation and evaporation are filled with NCEP data.

The global mean of SSM/I $\left(E - P - \frac{\partial W}{\partial t}\right)$ must be zero in order to solve Eq. (3) over the global domain since the area integral of $\nabla \bullet \mathbf{Q}_D$ of Eq. (3) over the global domain is zero. In order to satisfy the balance requirement for solving Eq. (3), the global mean biases are subtracted from the $\left(E - P - \frac{\partial W}{\partial t}\right)$ field to yield a zero global mean while preserving the spatial gradient of $\left(E - P - \frac{\partial W}{\partial t}\right)$. However, in the case of SSM/I, (1) water vapor divergences over the land are filled with NCEP values because SSM/I values are available only over the ocean; (2) adjustment is made only over the ocean to achieve a zero global mean by subtracting a fixed 0.67 mm day^{-1} from each SSM/I grid value over the ocean. The adjustment only over the ocean would result in a weaker SSM/I water vapor transport from the ocean to the land than without adjustment. The large positive adjustment in the SSM/I of 0.67 mm day^{-1} is due to larger evaporation than precipitation over the ocean, as indicated by the mean precipitation (2.5 mm day^{-1}) and mean evaporation rates (3.3 mm day^{-1}) averaged over the ocean.

In the reanalyses, however, water vapor transports are directly calculated from q and $\mathbf{V}$ data for more realistic depiction of water vapor transport rather than indirectly calculated from the $E - P$ field. It is because q and $\mathbf{V}$ fields are produced by assimilating the model outputs to various observations. In doing so, vertically integrated water vapor transport vectors ($\mathbf{Q}$) are obtained by applying Eq. (2) to reanalysis data, and then a similar methodology used for the SSM/I calculation is applied for calculating the potential function, i.e.:

$$\nabla \bullet \mathbf{Q} = -\nabla^2\Phi. \tag{5}$$

The same spherical harmonics approach is employed to avoid the boundary value problems for solving potential functions. The associated divergent component of water vapor transport ($\mathbf{Q}_D$) in the reanalsyes is then obtained by taking the gradient of potential function as in Eq. (4).

Examining the long-term water budget over the Asian monsoon domain, SSM/I-derived precipitation and total precipitable water (Wentz and Spencer 1998) for the May–September period of the years from 1988 to 2000 were obtained (from http://www.ssmi.com). The evaporation data were obtained from the products based upon an algorithm developed by Chou

(1993), in which the stability-dependent transfer coefficients were solved for the bulk aerodynamic formula iteratively, with latent, sensible, and momentum fluxes. Because SSM/I data were the main source for the evaporation retrieval, we refer to Chou's products as the SSM/I evaporation. Chou et al. (2003) validated the SSM/I daily evaporation data against various field experiment results. It has been reported that SSM/I daily evaporation products show the bias up to 0.09 mm day^{-1} with a correlation coefficient of 0.80 over the tropical oceans. The root mean square error (RMSE) on a monthly time scale was claimed to be about 0.19 mm day^{-1}, indicating a relatively small error ($\approx 6\%$) in comparison to the monthly mean evaporation rate of 3.21 mm day^{-1}.

The hydrological variables (i.e., E and P), specific humidity (q), and horizontal wind fields ($\mathbf{V}$) were obtained from the NCEP (Kalnay et al. 1996) and the ERA40 (Simmons and Gibson 2000) for a comparison with satellite-based results over the Asian summer monsoon region in the same 1988–2000 period. The NCEP reanalysis consists of 8 levels for q and 17 levels for $\mathbf{V}$, and for calculating the vertically integrated water vapor transport ($\mathbf{Q}$), only the lower 8 levels (1000, 925, 850, 700, 600, 500, 400, 300 hPa) of wind are used in conjunction with the q profiles. On the other hand, the ERA40 provides q and $\mathbf{V}$ at 23 levels from 1000 to 1 hPa, but only the lower 11 levels (1000, 925, 850, 775, 700, 600, 500, 400, 300, 250, 200 hPa) are used since most of the water vapor in the atmosphere resides below 200 hPa. In addition, we employed the Japanese 25-year Reanalysis Project (JRA25) data, from the ongoing cooperative project between the Japan Meteorological Agency (JMA) and the Central Research Institute of the Electric Power Industry (CRIEPI) for the target period of 1979–2004 (Onogi et al. 2005). The vertically integrated JRA25 water vapor fluxes are directly obtained from the JRA25 Web site (http://jra.kishou.go.jp).

3. Comparison of moisture flux divergence with radiosonde observation

We first compare satellite-estimated $\left(E - P - \frac{\partial W}{\partial t}\right)$ and moisture flux divergence ($\nabla \bullet \mathbf{Q}$) of reanalyses against $\nabla \bullet \mathbf{Q}$ from radiosonde observations. Also compared are between water vapor divergence from $E - P$ of reanalyses and that from q and $\mathbf{V}$ profiles of reanalyses. This comparison offers a way of examining the relative accuracy of the water budget derived from satellite measurements and reanalysis data, and of examining the calculation method for the flux divergence from reanalysis data.

Flux divergence from radiosonde observations is based on the line integral of the water vapor flux into the domain of interest. This method has been successfully implemented to calculate the vertically integrated moisture budget on a regional basis, such as over the Australian Gulf of Carpentaria (McBride et al. 1989). Green's theorem is applied over the domain, yielding the area mean moisture flux divergence over the domain:

$$\nabla \bullet \mathbf{Q} = \frac{1}{AREA}\int_{1000\,hPa}^{200\,hPa}\left(\oint q\mathbf{V}_n \bullet d\mathbf{l}\right)\frac{dp}{g} = E - P - \frac{\partial W}{\partial t}, \quad (6)$$

where q is the water vapor mixing ratio, $\mathbf{V}_n$ is the wind component normal to the boundary segment $d\mathbf{l}$, g is the acceleration of gravity, and $AREA$ is the domain area. Line integrals are performed along the boundaries of the domain at every 50 hPa level and vertical integration is done from 1000 to 200 hPa.

Two oceanic areas surrounded by radiosonde observation sites were chosen for the analysis (Fig. 1). Radiosonde observations were made at each site with 6-hourly soundings during the May–June 1998 period as a part of the Global Energy and Water cycle Experiment (GEWEX) Asian Monsoon Experiment (GAME), i.e., GAME/SCSMEX (South China Sea Monsoon Experiment)—see Lau et al. (2000) for the detailed information on this experiment. Vertically integrated water vapor fluxes onto two regions are obtained from daily averages of radiosonde data by applying Eq. (6) to enable the comparison with $\left(E - P - \frac{\partial W}{\partial t}\right)$ from SSM/I, and with the water vapor flux divergence ($\nabla \bullet \mathbf{Q}$) from reanalysis.

Figure 2 displays comparisons of SSM/I $\left(E - P - \frac{\partial W}{\partial t}\right)$ and NCEP, ERA40, and JRA25-derived moisture flux divergence ($\nabla \bullet \mathbf{Q}$) with the moisture flux divergence from radiosonde

Fig. 1. Two areas in the South China Sea where divergence of water vapor fluxes are computed from radiosonde data collected during the Intensive Observing Period (IOP) of the South China Sea Monsoon Experiment (SCSMEX) from May 1 to June 30, 1998.

observations over two regions in Fig. 1. Also compared are the $E-P$ of reanalyses against flux divergences ($\nabla \bullet \mathbf{Q}$) estimated from reanalyses q and $\mathbf{V}$ profiles.

On a daily basis, SSM/I-derived flux divergence is in good agreement with that suggested from radiosonde observations, showing a correlation coefficient of 0.88. The NCEP, ERA40, and JRA25 results based on the explicit moisture flux calculation in Eq. (2) show the correlation coefficients of 0.69, 0.67, and 0.75, respectively. Amongst three reanalyses, the JRA25 seems to have a largest mean bias although it holds highest correlation coefficient. The comparison of reanalysis $E-P$ with radiosonde-based flux divergence shows correlation coefficients of 0.67, 0.49, and 0.79 for NCEP, ERA40, and JRA25, respectively. Similar mean bias between $E-P$ and $\nabla \bullet \mathbf{Q}$ is found for JRA25. In general, the explicit calculation seems to result in flux divergences more comparable to radiosonde-derived values.

It is worthwhile to note that discrepancies are larger for reanalyses when radiosonde-derived convergence is large, reflecting the influence of few heavy rainfall events since the temporal and spatial variations of $E-P$ are predominantly controlled by variation in precipitation. In other words, water budget characteristics for heavy rain events during the summer over the experiment domain were well captured by radiosonde observations, but not well represented by NCEP, ERA40, and JRA25 precipitation. Those discrepancies for heavy rain events tend to be smaller when analyzed q and $\mathbf{V}$ fields are used for the flux divergence calculation, suggesting that the data assimilation brought into a better agreement with radiosonde-based water vapor divergence.

4. Properties of 13-year mean water vapor transport fields

Here thirteen year (1988–2000) summer (May–September) mean divergent component of water vapor transports are examined along with precipitation and evaporation over the Asian monsoon region. Since the SSM/I-derived products are available only over the ocean, the NCEP, ERA40, and JRA25 P and E are compared over the oceanic region of analysis domain.

4.1 Precipitation

Thirteen year (1988–2000) May–September (MJJAS) mean precipitation derived from the SSM/I and its differences from the reanalyses are shown in Fig. 3. The salient features found in the SSM/I precipitation (Fig. 3a) include heavy rainfall patterns located in the equatorial regions associated with strong convection in the monsoon trough extending from the Bay of Bengal to the Philippine Sea and the Intertropical Convergence Zone (ITCZ). High precipitation zones are also found in the equatorial eastern Indian Ocean slightly south of the equator and the South Pacific Convergence Zone (SPCZ). Also noted is the heavy precipitation along the East Asian subtropical front extending from the northern tip of the Philippines to the Kuroshio extension region along the northwest rim of the western Pacific Subtropical High. On the other hand, precipitation of less than 2 mm day^{-1} is seen over the subtropical Indian and the North Pacific Oceans, which are under the direct influence of the subsidence associated with the subtropical high pressure system.

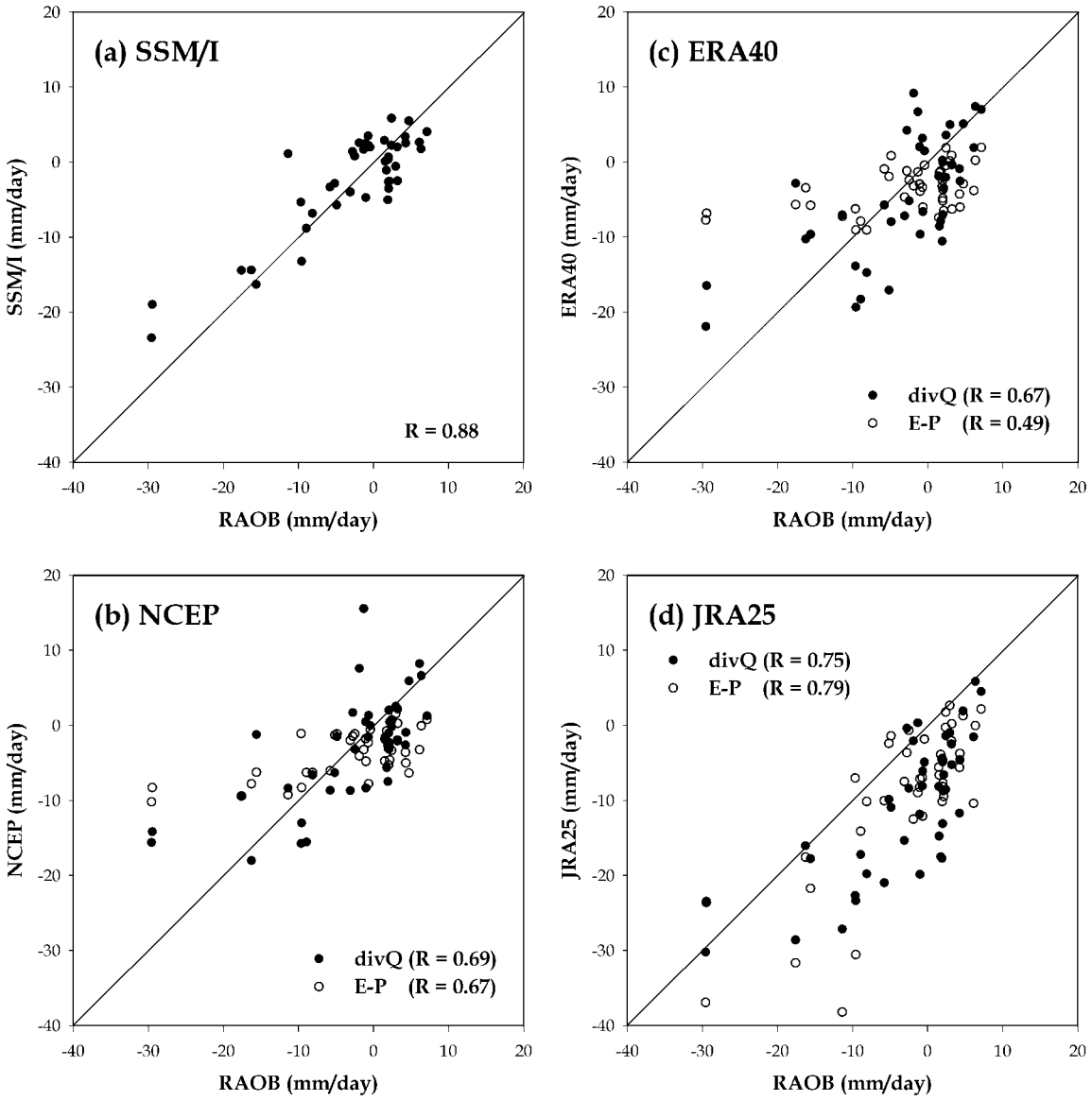

Fig. 2. Scatterplots for radiosonde-derived water vapor flux divergence vs. (a) SSM/I, (b) NCEP, (c) ERA40, and (d) JRA25-derived water vapor flux divergence, respectively. In (b)–(d), black and white dots indicate $\nabla \bullet \mathbf{Q}$ and $E - P$ of reanalyses, respectively.

Noticeable differences in precipitation exist among the three reanalyses and between the reanalyses and the satellite observation. One of the major differences is found over the East Asian subtropical front, extending from the East China Sea to the North Pacific, where significant underestimation of precipitation is found in all three reanalyses. By contrast, overestimates by reanalyses are commonly found over the North Pacific high area.

The NCEP (Fig. 3b) generally underestimates precipitation over the highly convective areas such as the equatorial Indian Ocean, the ITCZ along the equatorial western Pacific, and the East Asian monsoon region, whereas it overestimates over the drier regions such as

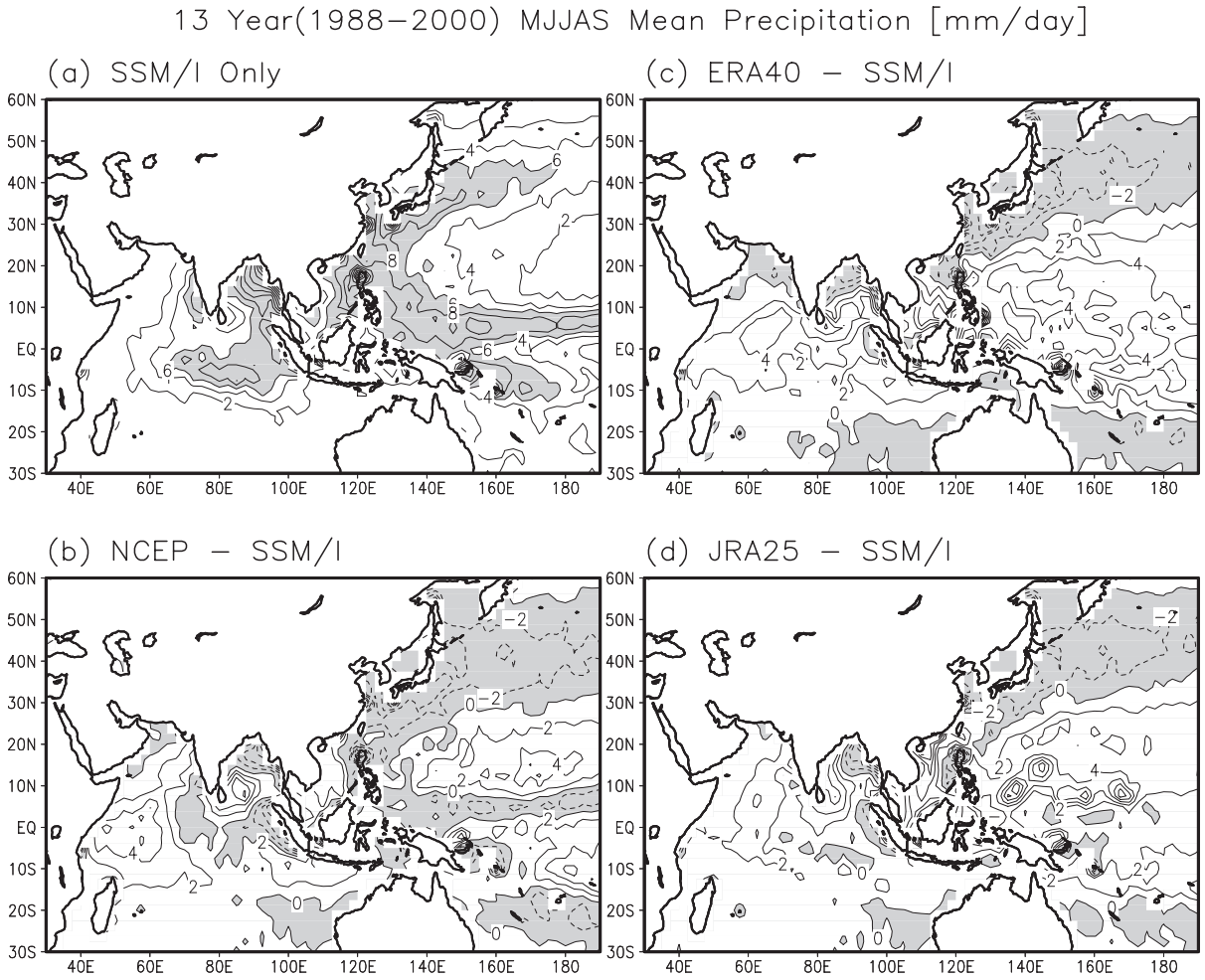

Fig. 3. Thirteen year (1988–2000) MJJAS mean (a) precipitation derived from SSM/I, and precipitation differences between SSM/I and (b) NCEP, (c) ERA40, and (d) JRA25. The contour intervals are 2 mm day^{-1}. Shaded area represents precipitation greater than 6 mm day^{-1} (a) and negative values (b–d).

subtropical oceans and the western Indian Ocean. The precipitation deficit along the ITCZ has been noted by Trenberth and Guillemot (1998), who pointed out that such a bias could be due to deficient precipitable water in the Tropics.

In contrast, the ERA40 in Fig. 3c shows an overestimation over most equatorial latitudes compared to SSM/I-derived precipitation. The largest discrepancies are found over the tropical western Pacific Ocean between 10°S and 20°N. This finding is consistent with the results of Bengtsson et al. (2004) who compared the ERA40 with two sets of precipitation climatology derived from the Global Precipitation Climatology Project (GPCP) and the CPC Merged Analysis of Precipitation (CMAP). This excessive precipitation over the Tropics seems due to the excessively strong circulation over the tropical convective regions in the ERA40 assimilation system (Hólm et al. 2002). Again, underestimation of precipitation is seen over the East Asian summer monsoon region.

While the difference pattern in the JRA25 (Fig. 3d) is similar to those of the NCEP and the ERA40, the magnitudes of the discrepancies in the JRA25 in the area off the east coast of Africa and over the equatorial western Indian Ocean are smaller. In general, the JRA25 shows better agreement with the SSM/I than

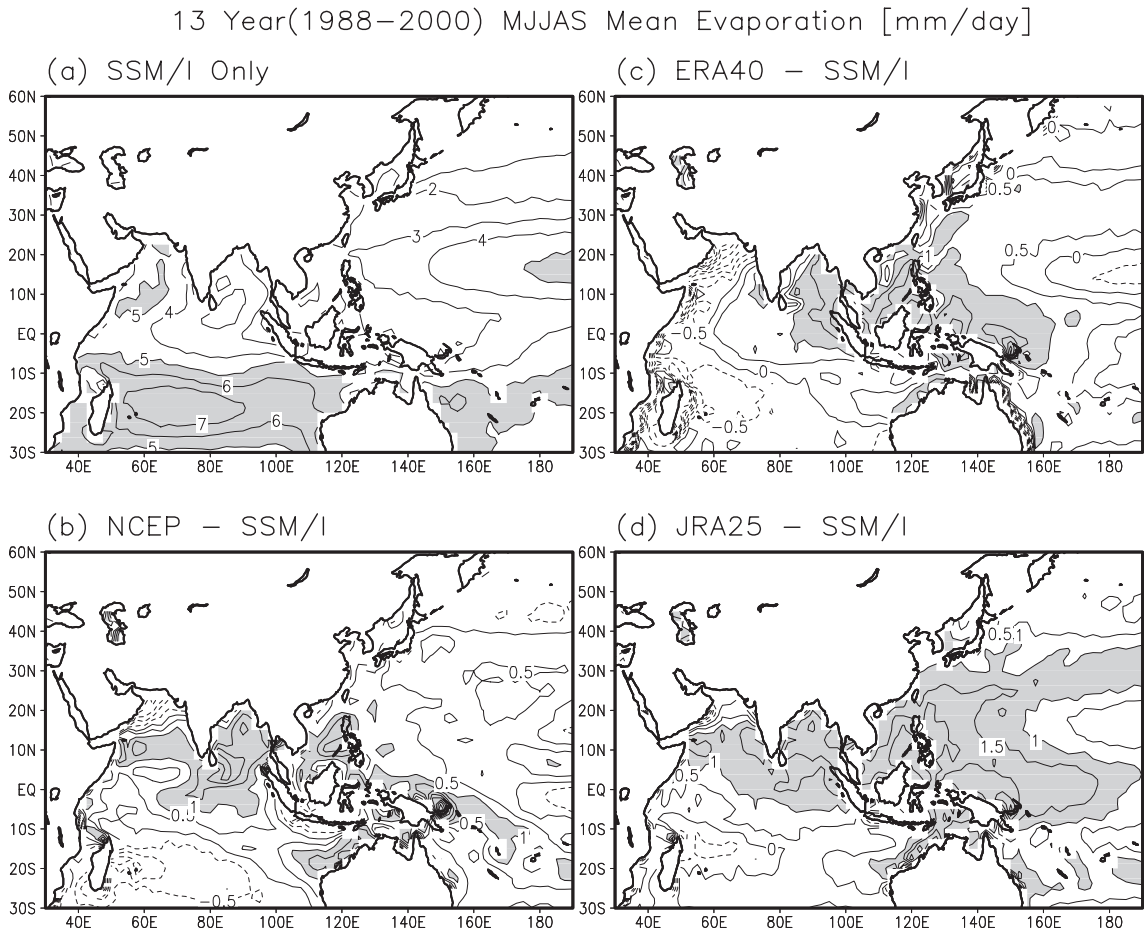

Fig. 4. Same as in Fig. 3 except for evaporation. The contour intervals are (a) 1 mm day^{-1} and (b)–(d) 0.5 mm day^{-1}, respectively. Shaded areas represent evaporation greater than (a) 5 mm day^{-1} and (b)–(d) 1 mm day^{-1}, respectively.

NCEP and ERA40 reanalysis do. The results of this comparison suggest that the long-term mean precipitation produced by the JRA25 in the Asian summer monsoon and the Indo-Pacific warm pool regions matches satellite observations better than those of the NCEP and the ERA40, even though all three reanalyses show significant underestimation of precipitation over the East Asian monsoon region.

4.2 Evaporation

The distributions of evaporation are given in Fig. 4. In the SSM/I distribution (Fig. 4a) values larger than 5 mm day^{-1} are found in the trade wind zone centered at about 20°S over the Indian and Pacific Oceans of the Southern Hemisphere. The reason is that in those regions high surface winds are coupled with a large surface humidity gradient (Chou et al. 2004; Feng and Li 2006). On the other hand, over the heavy precipitation areas, in particular in the equatorial oceans, evaporation rates are generally below about 4 mm day^{-1} probably due to the weak winds despite high surface air humidity over those regions. Relatively low evaporation is found in the Northern Hemisphere high latitudes because of the low sea surface temperature.

The seasonal mean distributions of evaporation fields reproduced by the NCEP, ERA40, and JRA25 are generally consistent with SSM/I estimations. However, significant differences are found in some regions. Figure 4b

shows that the NCEP evaporation is stronger than the SSM/I counterpart over the equatorial Indian Ocean and SPCZ. This is due to the fact that the effects of increased surface humidity gradients and moisture transfer coefficient override the effect of reduced surface winds in the NCEP (Chou et al. 2004). They further pointed out that the NCEP reanalysis system has a smaller surface humidity difference as well as a smaller moisture transfer coefficient over the rest of the area, especially in the southern Indian Ocean, which overrides the surface wind effect.

In the case of the ERA40 (Fig. 4c), the difference pattern in evaporation are qualitatively similar to that of the NCEP except for the western part of the Indian Ocean from Madagascar to the Arabian Sea, where lower evaporation is found in comparison to other reanalysis products. Larger evaporation over the western Pacific Maritime continent to the Bay of Bengal appears to be associated with larger surface humidity gradients in the ERA40 than the NCEP. Feng and Li (2006) asserted that the evaporation difference over the western Pacific is mainly due to the surface humidity difference rather than the surface wind magnitude.

On the other hand, the JRA25 shows greater evaporation rate over most of the tropical oceans, especially over the northern Indian Ocean and the tropical western Pacific (Fig. 4d). Apart from the NCEP and the ERA40, however, the analysis of surface humidity gradient versus wind speeds indicates that these spatial patterns can not be solely explained by the wind or humidity alone, rather, they are accounted for by the combined wind-humidity effect (not shown). The aforementioned results suggest that the details and accuracies of each variable in the bulk aerodynamic formula and the moisture transfer coefficients all contribute to improvement of the quality of evaporation.

4.3 *Divergent component of water vapor transports*

It is of interest to examine how the water vapor transports in reanalyses differ from SSM/I because water vapor transport implies energy transports shaping the atmospheric circulation pattern. Thirteen year (1988–2000) MJJAS mean potential function (Φ), divergent moisture flux ($\mathbf{Q}_D$), and its convergence ($\nabla \bullet \mathbf{Q}_D$) are presented in Fig. 5. In the SSM/I (Fig. 5a), the water vapor source (i.e., $\nabla \bullet \mathbf{Q}_D > 0$) regions are located over the Southern Hemisphere subtropical Indian and Pacific Oceans and the North Pacific Ocean, whereas sink regions (i.e., $\nabla \bullet \mathbf{Q}_D < 0$) are in the equatorial convective zones over the Pacific Ocean and the area from the western Pacific to the northeast of Japan along the rim of the western Pacific subtropical High, associated with the East Asian summer monsoon. The $\nabla \bullet \mathbf{Q}_D$ ($\approx E - P$) patterns are similar to those shown in precipitation. It is because precipitation behaves in a localized fashion while evaporation shows large-scale behavior, implying that spatial patterns of the vapor flux convergence (or divergence) are mainly controlled by the spatial distributions of precipitation. The resultant divergent water vapor transport ($\mathbf{Q}_D$) derived from the SSM/I is characterized by cross-equatorial transports from the Southern Hemisphere. These are consistent with well-known large-scale circulation features over the Asian summer monsoon region (Murakami and Matsumoto 1994; Li and Yanai 1996; Sohn et al. 2001); i.e., (1) the cross-equatorial flow associated with monsoon circulation over the Indian Ocean, (2) the southeast flow associated with the anticyclonic circulation over the western Pacific, and (3) the cross-equatorial flow north of New Guinea. These transports then result in a strong water vapor convergence over the Bay of Bengal, the tropical western Pacific, and the East Asian monsoon region.

The general features of moisture transports from the three reanalyses are in good agreement with those from SSM/I; however, significant differences are found in some areas (see Figs. 5b–d). The common features found in the three reanalyses are significantly weaker northwestward transports over the Pacific Ocean north of 10°N, in comparison to SSM/I. Thus, the strong convergence over the East Asian monsoon region, from northern Philippines to east of Japan noted in SSM/I, is not well depicted in the three reanalyses. In the case of NCEP (Fig. 5b), the magnitudes of the potential function and moisture transports are substantially smaller than those of SSM/I over the entire oceanic area, indicating weak moisture convergence and divergence in the

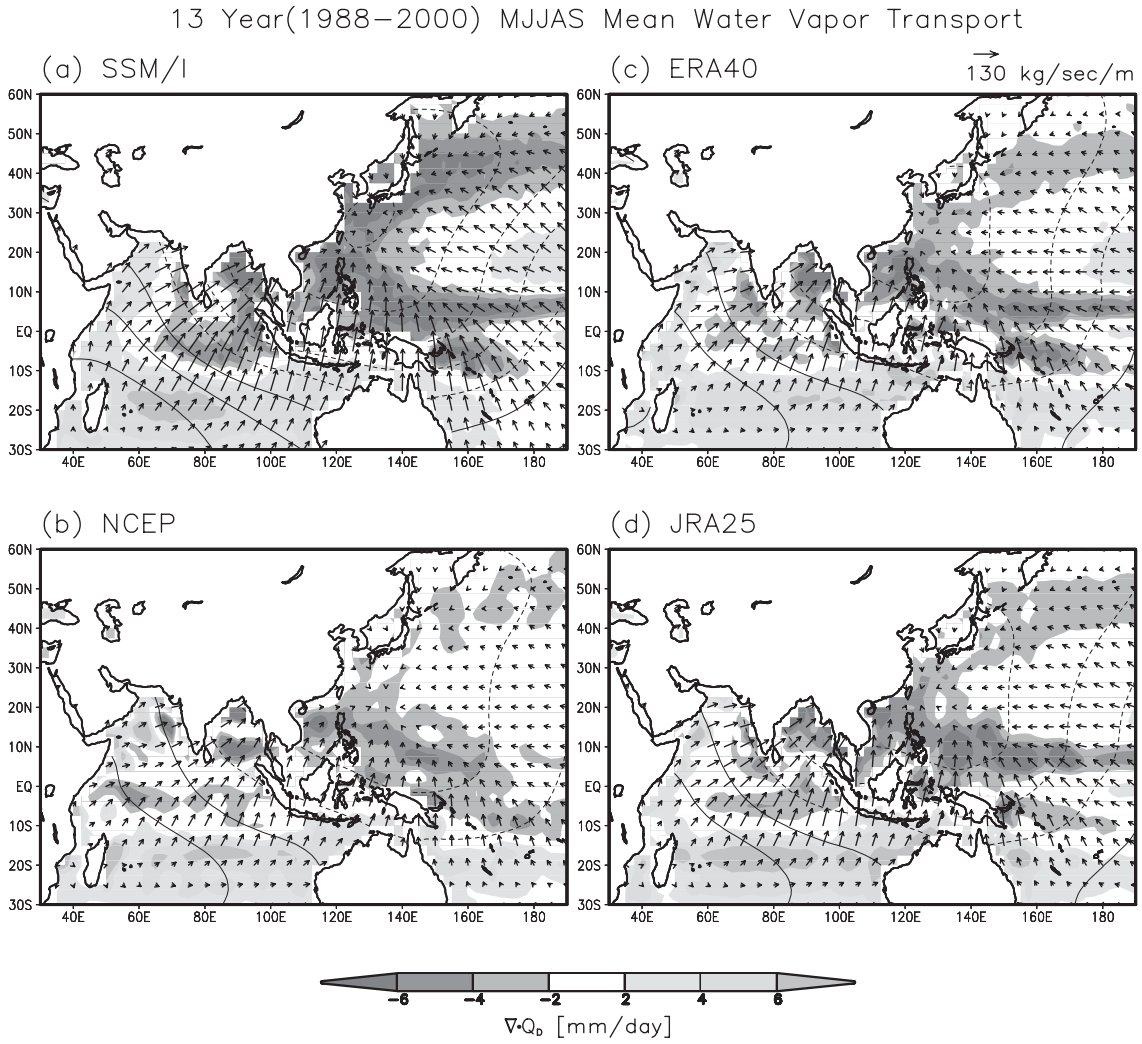

Fig. 5. Thirteen year (1988–2000) MJJAS mean divergent component of water vapor transports [$\mathbf{Q}_D$] (arrow) derived from (a) SSM/I, (b) NCEP, (c) ERA40, and (d) JRA25, respectively. The contours indicate the water vapor transport potential function [Φ] with the intervals in 1.0×10^8 kg s^{-1}. $\nabla \bullet \mathbf{Q}_D$ is shown in shaded area with the intervals in 2 mm day^{-1}.

NCEP. No distinct moisture convergence regions are found in the equatorial regions from the Bay of Bengal to the Philippine Sea, the Intertropical Convergence Zone (ITCZ) over the equatorial western Pacific, the South Pacific Convergence Zone (SPCZ), and the East Asian monsoon region along the northwest rim of the western Pacific Subtropical High, where strong water flux convergences are noted in the SSM/I.

On the other hand, the magnitude of moisture transports of the ERA40 is larger than those of NCEP, but substantially smaller than suggested from SSM/I (Fig. 5c) although the general patterns of flux convergence are quite similar to SSM/I. In contrast much similar patterns as well as magnitudes are found between the ERA40 and the JRA25 (Fig. 5c and Fig. 5d).

Summarizing the different features discussed for Fig. 5, the 13 year (1988–2000) MJJAS mean Φ, $\mathbf{Q}_D$, and $\nabla \bullet \mathbf{Q}_D$ differences between the SSM/I and three reanalyses are shown in Fig. 6. The difference map between NCEP and SSM/I (i.e., NCEP minus SSM/I) depicts additional southward moisture transports over the

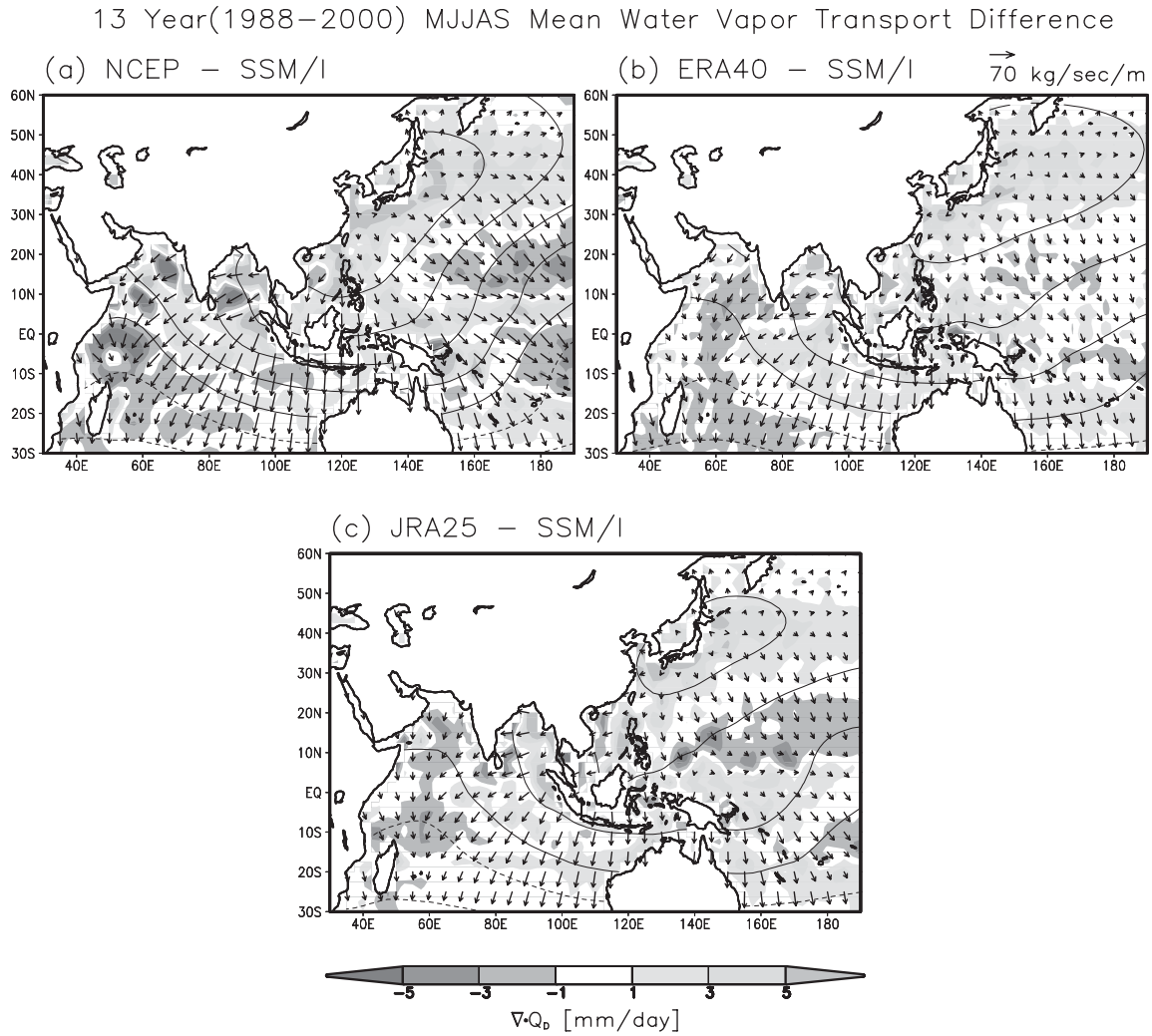

Fig. 6. Thirteen year (1988–2000) MJJAS mean divergent component of water vapor transport [$\mathbf{Q}_D$] differences between SSM/I and (a) NCEP, (b) ERA40, and (c) JRA25, respectively (arrow). The contours indicate differences of the water vapor transport potential function [Φ] with the intervals 0.5×10^8 kg s^{-1}. Differences of $\nabla \bullet \mathbf{Q}_D$ are shown in the shaded area with the intervals in 2 mm day^{-1}.

entire ocean, implying that the NCEP produces weaker northeastward transport over the Indian Ocean and northwestward transport over the Pacific Ocean compared with the SSM/I—Fig. 6a. On the other hand, the ERA40 minus SSM/I (Fig. 6b) shows smaller spatial gradients of Φ fields over most of the Indian Ocean, suggesting that the ERA40 moisture transports over the Indian Ocean more resemble those inferred from SSM/I. It is noted that differential southward transports are prevalent over the southern hemispheric Indian and Pacific Oceans, indicating that northward transports in the ERA40 are much weaker over those oceanic areas than those inferred from SSM/I. The JRA25 (Fig. 6c) also shows very similar differential patterns to those in the ERA40, resulting in weaker northward water vapor transports over the southern hemispheric oceans and weaker northwestward transports over the North Pacific.

5. Water vapor transports in the climatological intraseasonal variation

One of dominant phenomena over the Asian monsoon regions is the climatological intra-

seasonal oscillations (CISO) (Nakazawa 1992; Wang and Xu 1997; Kang et al. 1999; LinHo and Wang 2002). The CISO, which differs from transient intraseasonal oscillation such as the Madden-Julian Oscillation (Madden and Julian 1971), results from phase-lock to the seasonal cycle of the transient intraseasonal variation. It may be viewed as a result of the regulation of the transient intraseasonal oscillation by the annual cycle (Wang and Xu 1997). It is well known that because of the intraseasonal oscillation, the South Asian summer monsoon exhibits substantial subseasonal variability, often referred to as the active/break phases of the monsoon. The intraseasonal variations in the East Asian monsoon region are best reflected into the northward migration of the major subtropical rain band. The latter is directly connected to the convergence or divergence of water vapor transport over the East Asian region. Thus, it is of great interest to examine how the climatological intraseasonal oscillation of water vapor transports from reanalysis products compare with SSM/I-inferred features in the Asian monsoon region. In doing so we use the 20–95 day filtered data because there are various intraseasonal time scales [e.g., 20–80 days (Lau and Yang 1996) and 15–95 days (Jiang et al. 2004)], being dominant in the Indian and East Asian monsoon regions.

Examining the latitudinal changes with time over the Indian monsoon region, $\nabla \bullet \mathbf{Q}_D$ was averaged over the (80°–90°E) belt and is presented as the time-latitude diagrams in Fig. 7. The SSM/I water vapor divergence field shows that there is an alternating divergence and convergence of water vapor mainly over the ocean from 10°S to 20°N (Fig. 7a), with northward moving patterns. From May to September, four dominant northward propagating moisture convergence (divergence) cycles are noted, at about 30-day time intervals.

The latitude-time evolutions of the 20–95 day filtered water vapor flux divergence over the 80°–90°E longitude were also obtained from three reanalyses—see Figs. 7b–d. The CISO patterns from 10°S to 20°N shown in NCEP (Fig. 7b) are in general agreement with those from SSM/I, clearly showing the features of northward propagation. But the signals are much weaker in comparison to what is suggested from SSM/I. Furthermore, the signals appearing in SSM/I over the equatorial latitudes are not clear in the NCEP reanalysis products.

The ERA40 (Fig. 7c) also exhibits well-defined northward propagating features of vapor flux divergence/convergence, similar to those noted in the SSM/I. It can be seen that the spatial and temporal patterns of the CISO in the region between 10°S and 20°N are clearer than those in NCEP throughout the analysis period. Nonetheless the magnitudes are still much smaller when compared with SSM/I.

As shown in the 13 year mean water vapor transports, the JRA25 (Fig. 7d) appears to have similar CISO patterns to those in the ERA40. In particular, a strong divergence region propagating from 10°S to 30°N, in the period from mid June to late July, is similar to the ERA40, although such a pattern is not shown in SSM/I. Less prominent CISO signal propagating northward is found during May and in the period from late July to August. The magnitudes of flux divergence in JRA25 appear to be weaker than those of SSM/I, but similar to the ERA40.

Comparisons of water vapor flux divergences ($\nabla \bullet \mathbf{Q}_D$) were also made over the East Asian monsoon region. In doing so, flux divergences were averaged over the 125°–135°E longitude belt and the results are given as time-latitude diagrams in Fig. 8. It shows that the CISO signals of water vapor flux divergence are also evident over the East Asian region. In the SSM/I (Fig. 8a), the northward propagating CISO signals appear to extend from 5°S to 40°N during the summer. Three dominant northward propagating moisture convergence (divergence) cycles are found during the May–September period. From May to mid-July a strong moisture convergence area propagates northward from 10°N to 40°N latitude. The next convergence area propagates north from about the equator to 40°N during the early July-late August period. The third one seems to propagate from mid-August to late September with a comparatively weak magnitude. Among those three northward moving convergence patterns, the first one seems to be related to the evolution of the East Asian monsoon rain band associated with the Mei-Yu and Baiu around mid-

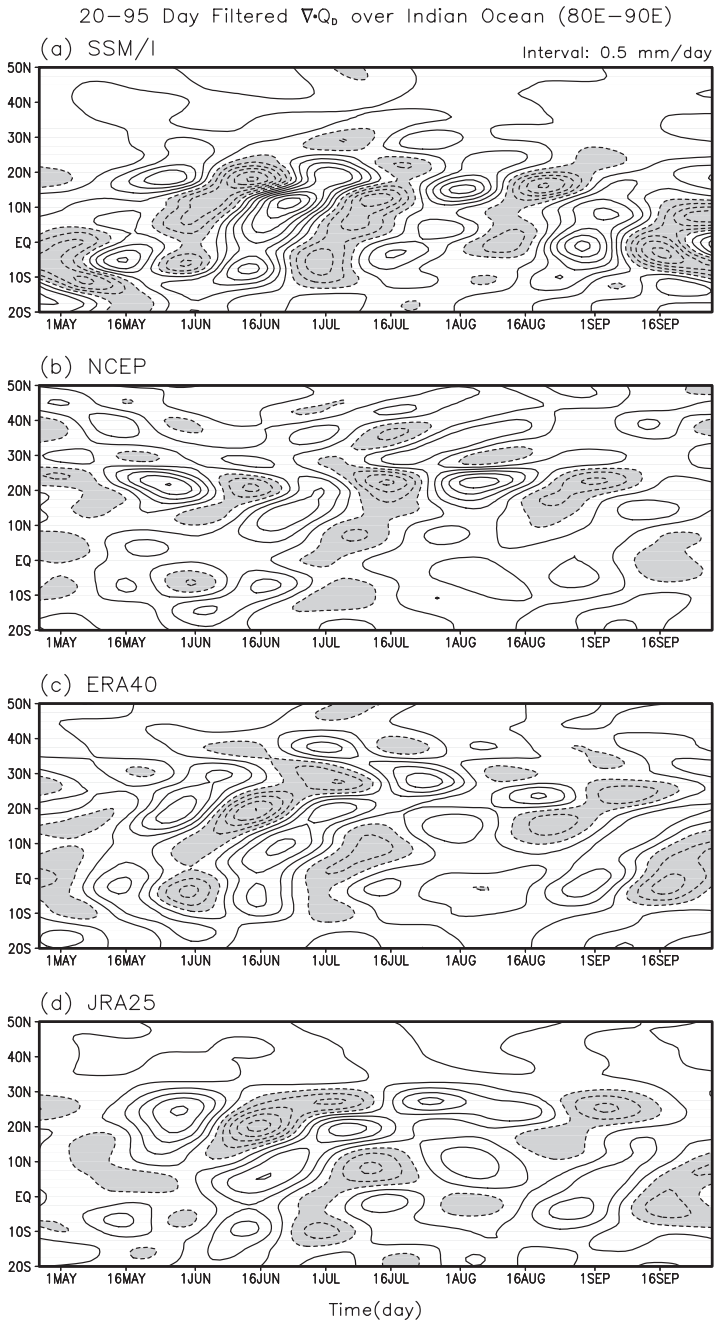

Fig. 7. The Hovmöller diagram of $\nabla \bullet \mathbf{Q}_D$ for (a) SSM/I, (b) NCEP, (c) ERA40, and (d) JRA25. Values were averaged in the longitudinal belt from 80°E to 90°E. The contour interval is in 0.5 mm day^{-1} and the shaded area represents $\nabla \bullet \mathbf{Q}_D$ less than -0.5 mm day^{-1}.

June and the Changma in late June (Lau and Li 1984; Lau et al. 1988; Sohn et al. 2001). It has been known that along the longitude band 122.5°–132.5°E there are four major episodes of northward propagation of outgoing longwave radiation (OLR) anomalies from May to October (Wang and Xu 1997). Among those four episodes, the first three occur in the May to September period, and are consistent with those described in the SSM/I.

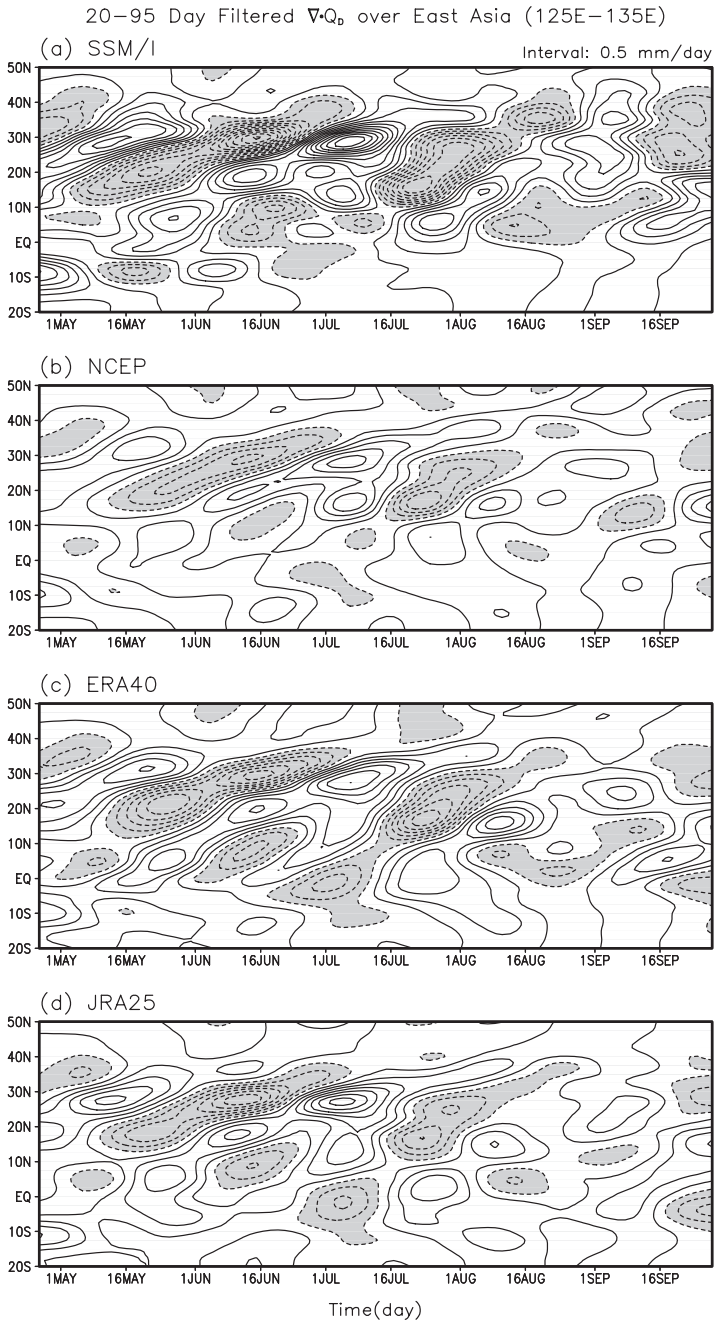

Fig. 8. Same as in Fig. 7 except for averaged from 125°E to 135°E.

Similar features of the CISO are found in the NCEP along the latitude from 10°N to 40°N (Fig. 8b). However, the moisture flux divergence and convergence are much smaller compared to the SSM/I values. The general features of the CISO in both ERA40 and JRA25 are similar to each other and are in good agreement with those of SSM/I (Figs. 8c–d), although the JRA25 CISO signal tends to be weaker than ERA40. Three dominant northward propagating moisture convergence (divergence) cycles are clearer than those in NCEP, but both ERA40 and JRA25 show relatively weak northward propagating signals compared

with SSM/I values. In particular, weak signals are evident in the later part of August and during September. These weak signals may be in part due to characteristic differences between satellite observation and reanalysis. Since this period is subject to large interannual variability of typhoon-related precipitation, reanalysis may not well represent such mesoscale heavy rain events that can be well depicted by satellite observations.

It should be noted that the CISO signals derived from a 13-year climatology should be rigorously tested. In Wang and Xu (1997) (WX97 hereafter), three statistical methods (sign test, *t*-test, and Monte Carlo test) were applied to show the statistical significance of the CISO derived by a 17-year mean OLR annual cycle. Further, they showed that the CISO revealed by OLR has a coherent dynamic structure with the CISO derived from NCEP reanalysis. The four CISO cycles during May to October detected in WX97 have been confirmed later by using longer climatological data sets (Wang et al. 2005). While the statistical test was not repetitively performed here, the consistence between the SSM/I derived moisture flux convergence and the results of WX97 derived from OLR and wind fields lends support to the credibility of the SSM/I analysis here.

In summary, it is shown that the moisture convergence and divergence from SSM/I measurements clearly depict northward propagating features in the CISO time scales over the Indian summer monsoon region as well as in the East Asian monsoon region. The NCEP, ERA40, and JRA25 reanalyses show northward propagating features similar to those found in the SSM/I; however, the magnitudes of moisture flux divergence/convergence in the three reanalyses appear to be generally weak. Amongst three reanalyses, the ERA40 seems to be most comparable to the SSM/I.

6. Summary and conclusions

Water cycle parameters (precipitation, evaporation, and water vapor transport) in the atmospheric branch from NCEP, ERA40, and JRA25 reanalysis were compared with SSM/I-derived estimates over the Asian summer monsoon region, in terms of moisture sources and sinks, and their associated transport features. Satellite-derived SSM/I products were considered to be a reference for the comparison. We have identified the common features and discrepancies among various reanalyses and satellite-based results, and explained why such discrepancies may exist.

In the 13 year (1988–2000) MJJAS mean climatology from the SSM/I, the water vapor source regions are located over the subtropical Indian and Pacific Oceans in the Southern Hemisphere, and over the North Pacific Ocean. On the other hand, moisture sink regions are located in the Asian monsoon trough, the equatorial convective zones over the Pacific Ocean and the East Asian monsoon region from the northern Philippines to east of Japan. Thus, the resultant divergent water vapor transport ($\mathbf{Q}_D$) is characterized by cross-equatorial transports of water vapor from the subtropical oceans in the Southern Hemisphere and water vapor transports along the southwestern boundary of the North Pacific high. These are consistent with well-known large-scale circulation features over the Asian summer monsoon region, i.e., (1) the cross-equatorial flow associated with monsoon circulation over the Indian Ocean, (2) the southeast flow over the tropical western North Pacific, and (3) cross-equatorial flow from the east of Australia. In conjunction with these water vapor sources and sinks, the climatological intraseasonal variations of the moisture flux convergence over the Asian summer monsoon regions clearly show northward propagating patterns in the South Asia and the East Asian sectors.

The general long-term summer mean features found in all three reanalyses are in good agreement with those from SSM/I; however, much weaker northwestward transports over the Pacific Ocean north of 10°N are found in comparison to SSM/I. Thus, the strong convergence over the East Asian monsoon region from the western Pacific to the east of Japan shown in SSM/I is not well described in any of three reanalyses. The salient findings are summarized as follows:

(1) NCEP

In the summer mean climatology, the magnitudes of the moisture transports are much smaller than those of SSM/I over the whole ocean area, and thus indicate weaker moisture convergence and divergence. It is also shown

that the CISO magnitudes are much weaker, even though the northward propagating patterns are similar to those found in the SSM/I over the Asian summer monsoon region.

(2) ERA40

The magnitudes of the moisture transports shown in the summer mean climatology are comparable to those of SSM/I. General patterns of flux convergence are quite similar to SSM/I. The CISO patterns are also similar to those in SSM/I, and magnitudes of the northward propagating signals are more comparable to SSM/I, in comparison to NCEP and JRA25 reanalyses.

(3) JRA25

The JRA25 is much similar to the ERA40 in its spatial patterns as well as in the magnitude of its divergent component of water vapor transports. The northward moving patterns of CISO are also similar to the ERA40 over the Asian summer monsoon region.

It is important that the reanalysis products, particularly hydrological variables such as precipitation and evaporation, and moisture flux divergence, are compared and assessed against satellite-based observations or some other ground-based observations. This paper presents a new effort to describe the mean features of divergent components of water vapor transport and its climatological intraseasonal variation over the Asian summer monsoon region from a satellite-based observational approach.

The ramification of the results here is far reaching. It implies that the water vapor budget drawing upon the reanalysis datasets may have considerable uncertainties. Caution should be exercised when quantitative assessment is attempted. In a recent analysis of the water vapor budget in the East Asian summer monsoon region (10°N–50°N, 90°E–145°E) for the period of May–August 1998, Wang and Yang (2006) found that the moisture transport from the Bay of Bengal and from the Philippine Sea into the East Asian domain differ by 20–30% between the NCEP/DOE reanalysis-2 and the ERA40 datasets; further, the total moisture convergence into the East Asian summer monsoon domain differ by 47% between the two reanalyses. These uncertainties result in remarkable uncertainties in the regional climate modeling of the East Asian summer monsoon in which the regional climate model solution critically relies on the large scale lateral boundary forcing fields.

Acknowledgements

The authors would like to thank Dr. Yuki Honda of the Japan Meteorological Agency, the editor of the JMSJ, and two anonymous reviewers for their constructive and valuable comments which led to improvements in the quality of the paper. This research has been supported by the SRC program of the Korea Science and Engineering Foundation, and also by the BK21 Project of the Korean Government. This research was partially performed while the first author was resident at the International Pacific Research Center, University of Hawaii at Manoa. Bin Wang acknowledges the support from the International Pacific Research Center which is in part supported by the Frontier Research Center for Global Changes. The authors wish to thank NCEP/NCAR and ECMWF for releasing reanalysis data. The JRA25 data were obtained from the Japanese 25-year Reanalysis Project Web site (http://jra.kishou.go.jp).

References

Annamalai, H., J.M. Slingo, K.R. Sperber, and K. Hodges, 1999: The mean evolution and variability of the Asian summer monsoon: Comparison of ECMWF and NCEP-NCAR reanalyses. *Mon. Wea. Rev.*, **127**, 1157–1186.

Bengtsson, L., K.I. Hodges, and S. Hagemann, 2004: Sensitivity of large-scale atmospheric analyses to humidity observations and its impact on the global water cycle and tropical and extratropical weather systems in ERA40. *Tellus*, **56A**, 202–217.

Chen, T.C., 1985: Global water vapor flux and maintenance during FGGE. *Mon. Wea. Rev.*, **113**, 1801–1919.

Chou, S.H., 1993: A comparison of airborne eddy correlation and bulk aerodynamic methods for ocean-air turbulent fluxes during cold-air outbreaks. *Bound.-Layer Meteor.*, **64**, 75–100.

Chou, S.H., E. Nelkin, J. Ardizzone, and R.M. Atlas, 2004: A comparison of latent heat fluxes over global oceans for four flux products. *J. Climate*, **17**, 3973–3989.

Chou, S.H., E. Nelkin, J. Ardizzone, R.M. Atlas, and C.L. Shie, 2003: Surface turbulent heat and

momentum fluxes over global oceans based on the Goddard Satellite Retrievals, Version 2 (GSSTF2). *J. Climate*, **16**, 3256–3273.

Cohen, J.L., D.A. Salstein, and R.D. Rosen, 2000: Interannual variability in the meridional transport of water vapor. *J. Hydrometeor.*, **1**, 547–553.

Feng, L. and J. Li, 2006: A comparison of latent heat fluxes over global oceans for ERA and NCEP with GSSTF2. *Geophys. Res. Lett.*, **33**, 10.1029/2005GL024677.

Hólm, E., E. Andersson, A. Beljaars, P. Lopez, J.F. Mahfouf, A. Simmons, and J.N. Thépaut, 2002: Assimilation and Modeling of the Hydrological Cycle: ECMWF's Status and Plans, ECMWF Technical Report 383. ECMWF, Reading, UK.

Jiang, X., T. Li, and B. Wang, 2004: Structures and mechanisms of the northward propagating boreal summer intraseasonal oscillation. *J. Climate*, **17**, 1022–1039.

Kalnay, E. and Coauthors, 1996: The NCEP/NCAR 40-year reanalysis project. *Bull. Amer. Meteor. Soc.*, **77**, 437–471.

Kang, I.S., C.H. Ho, Y.K. Lim, and K.M. Lau, 1999: Principal modes of climatological seasonal and intraseasonal variations of the Asian summer monsoon. *Mon. Wea. Rev.*, **127**, 322–340.

Lau, K.M. and M.T. Li, 1984: The monsoon of East Asia and its global associations-A survey. *Bull. Amer. Meteor. Soc.*, **65**, 114–125.

Lau, K.M., G.J. Yang, and S.H. Shen, 1988: Seasonal and intraseasonal climatology of summer monsoon rainfall over East Asia. *Mon. Wea. Rev.*, **116**, 18–37.

Lau, K.M. and S. Yang, 1996: Seasonal variation, abrupt transition, and intraseasonal variability associated with the Asian summer monsoon in the GLA GCM. *J. Climate*, **9**, 965–985.

Lau, K.M. and coauthors, 2000: A report of the field operations and early results of the South China Sea Monsoon Experiment (SCSMEX). *Bull. Amer. Meteor. Soc.*, **81**, 1261–1270.

Li, C. and M. Yanai, 1996: The onset and interannual variability of the Asian summer monsoon in relation to land-sea thermal contrast. *J. Climate*, **9**, 358–375.

LinHo. and B. Wang, 2002: The time-space structure of the Asian-Pacific summer monsoon: A fast annual cycle view. *J. Climate*, **15**, 2001–2019.

Madden, R.A. and P.R. Julian, 1971: Detection of a 40–50 day oscillation in the zonal wind in the tropical Pacific. *J. Atmos. Sci.*, **28**, 702–708.

McBride, J.L., B.W. Gunn, G.J. Holland, T.D. Keenan, N.E. Davidson, and W.M. Frank, 1989: Time series of total heating and moistening over the Gulf of Carpentaria radiosonde array during AMEX. *Mon. Wea. Rev.*, **117**, 2701–2713.

Mo, K.C. and R.W. Higgins, 1996: Large-scale atmospheric moisture transport as evaluated in the NCEP/NCAR and the NASA/DAO reanalyses. *J. Climate*, **9**, 1531–1545.

Murakami, T. and J. Matsumoto, 1994: Summer monsoon over the Asian continent and western North Pacific. *J. Meteor. Soc. Japan*, **72**, 719–745.

Nakazawa, T., 1992: Seasonal phase lock of intraseasonal oscillation during the Asian summer monsoon. *J. Meteor. Soc. Japan*, **70**, 597–611.

Newman, M., P.D. Sardeshmukh, and J.W. Bergman, 2000: An assessment of the NCEP, NASA, and ECMWF reanalyses over the tropical west Pacific warm pool. *Bull. Amer. Meteor. Soc.*, **81**, 41–48.

Onogi, K., H. Koide, M. Sakamoto, S. Kobayashi, J. Tsutsui, H. Hatsushika, T. Matsumoto, N. Yamazaki, H. Kamahori, K. Takahshi, K. Kato, T. Ose, S. Kadokura, and K. Wada, 2005: JRA-25: Japanese 25-year re-analysis project-progress and status. *Quart. J. Roy. Meteor. Soc.*, **131**, 3259–3268.

Rasmusson, E.M. and K.C. Mo, 1996: Large-scale atmospheric moisture cycling as evaluated from NMC global analysis and forecast products. *J. Climate*, **12**, 3276–3297.

Roads, J., M. Kanamitsu, and R. Stewart, 2002: CSE Water and energy budgets in the NCEP-DOE reanalysis II. *J. Hydrometeor.*, **3**, 227–248.

Rosen, R.D., D.A. Salstein, and J.P. Peixoto, 1979: Variability in the annual fields of large-scale atmospheric water vapor transport. *Mon. Wea. Rev.*, **107**, 26–37.

Simmons, A.J. and J.K. Gibson, 2000: The ERA-40 project plan, ERA-40 Project Report Series No. 1, ECMWF, Reading, UK, 62 pp.

Sohn, B.J., H.S. Chung, D.H. Kim, D. Perkey, F.R. Robertson, and E.A. Smith, 2001: Use of satellite-derived water vapor data to investigate northwestward expansion of North Pacific subtropical high during 1995 summer. *J. Meteor. Soc. Japan*, **79**, 1059–1075.

Sohn, B.J., E.A. Smith, F.R. Robertson, and S.C. Park, 2004: Derived over-ocean water vapor transports from satellite-retrieved $E - P$ datasets. *J. Climate*, **17**, 1352–1365.

Trenberth, K.E. and C.J. Guillemot, 1995: Evaluation of the global moisture budget as seen from analyses. *J. Climate*, **8**, 2255–2272.

Trenberth, K.E. and C.J. Guillemot, 1998: Evaluation of the atmospheric moisture and hydrological cycle in the NCEP/NCAR reanalyses. *Clim. Dyn.*, **14**, 213–231.

Wang, B. and X. Xu, 1997: Northern Hemisphere

summer monsoon singularities and climatological intraseasonal oscillation. *J. Climate*, **10**, 1071–1085.

Wang, B., T. Li, Y. Ding, and R. Zhang, 2005: East Asian–western North Pacific monsoon: A distinct component of the Asian-Australian monsoon system. In "*The Global monsoon System: Research and Forecast*", Ed. C.-P. Chang, B. Wang, and G. Lau, World Meteorological Organization, WMO TD number 1266, pp 545.

Wang, B. and H. Yang, 2006: Hydrological issues in the regional modeling of the East Asian summer monsoon. Submitted to *Clim. Dyn.*

Wentz, F.J. and R.W. Spencer, 1998: SSM/I rain retrievals within a unified all-weather ocean algorithm. *J. Atmos. Sci.*, **55**, 1613–1627.